RESEARCH ARTICLE

MRI-determined carotid artery flow velocities and wall shear stress in a mouse model of vulnerable and stable atherosclerotic plaque

**Glenda S. van Bochove · Roel Straathof ·
Rob Krams · Klaas Nicolay · Gustav J. Strijkers**

Abstract

Objectives We report here on the pre-clinical MRI characterization of an apoE−/− mouse model of stable and vulnerable carotid artery atherosclerotic plaques, which were induced by a tapered restriction (cast) around the artery. Specific focus was on the quantification of the wall shear stress, which is considered a key player in the development of the plaque phenotype.

Materials and methods In vivo MRI was performed at 9.4 T. The protocol consisted of time-of-flight angiography, high-resolution T1- and T2-weighted black-blood imaging and phase-contrast flow velocity imaging as function of time in the cardiac cycle. Wall shear stress was determined by fitting the flow profile to a quadratic polynomial.

Results Time-of-flight angiography confirmed preservation of blood flow through the carotid arteries in all cases. T1- and T2-weighted MRI resulted in high-resolution images in which the position of the cast, luminal narrowing introduced by cast and plaque, as well as the arterial wall could be well identified. Laminar flow with low wall shear stress (11.2 ± 5.2 Pa) was measured upstream to the cast at the position of the vulnerable plaque. Downstream to the cast at the position of the stable plaque, the apparent velocities were low, which

is consistent with vortices and an oscillatory nature of the flow.

Conclusions Flow velocities and wall shear stress were successfully measured in this mouse model of stable and unstable plaque. The presented tools can be used to provide valuable insights in the pathogenesis of atherosclerosis.

Introduction

The pathogenesis of atherosclerosis is a complex process, with genetic predisposition, diet and lifestyle as contributing factors. Atherosclerosis displays a focal pattern, occurring predominantly at curvatures and branches of the vascular tree, which provides support to the hypothesis that local blood flow patterns play a role in the development of atherosclerosis. The local hemodynamic conditions, such as the flow velocity, wall shear stress and arterial wall compliance, are known to influence the endothelial biological function. High shear stresses with a well-defined constant direction are found to be atheroprotective, as the endothelial cells are able to remodel in a controlled way to maintain the vascular homeostasis. On the other hand, low and oscillatory shear stresses in regions of complex geometry, e.g., near bifurcations of arteries, are pro-atherogenic and cause molecular signaling of pro-inflammatory pathways [1]. Several studies showed a clear relationship between the presence of atherosclerotic plaque in humans and animals at sites of altered wall shear stress [2–4].

Recently, Cheng et al. [5] have introduced a new technique, which allows for the controlled study of the influence of wall shear stress on the development of atherosclerosis.

G. S. van Bochove · R. Straathof · K. Nicolay · G. J. Strijkers (✉)
Biomedical NMR, Department of Biomedical Engineering,
Eindhoven University of Technology, PO Box 513,
5600 MB Eindhoven, The Netherlands
e-mail: g.j.strijkers@tue.nl

R. Krams
Department of Bioengineering, London Imperial College,
London, UK

The method involves the placement of an innovative tapered restriction (cast) surgically placed around the right common carotid artery of an apoE−/− mouse on a lipid-rich diet. Upstream to the cast (toward the heart), a region of lowered wall shear stress induced a lesion with characteristics of a vulnerable plaque, i.e., high macrophage, high lipid and low collagen content, while downstream to the cast, oscillatory wall shear stress resulted in a lesion with characteristics of a stabilized plaque, i.e., lower lipid and higher collagen content. This model provides evidence that the local hemodynamics not only lies at the basis of the development of plaque but also is implicated in plaque phenotype.

Pre-clinical MRI plays a significant role in the study of experimental atherosclerosis. Currently, MRI is capable of detecting luminal narrowing, plaque size and morphology with high accuracy and reproducibility, providing reliable indices of plaque burden. With the progress in the design of targeted MRI contrast agents (molecular imaging) aimed at discriminating vulnerable from stable plaque phenotypes [6], there is great need for animal models of controlled plaque phenotype. The mouse model recently introduced by Cheng et al. is particularly suitable for that purpose.

The aim of this study was to characterize the above apoE−/− mouse model using pre-clinical high-field MRI. High-resolution black-blood T1- and T2-weighted imaging were used to depict the exact position of the cast and the size of the carotid artery lumen. Three-dimensional time-of-flight angiography was used to image the vascular tree and to confirm preservation of blood flow through the cast placed around the right carotid artery. Finally, high-resolution phase-contrast velocity imaging was used to measure maximum flow velocities and wall shear stress in the left and right carotid arteries.

Materials and methods

Mouse model

The local institutional animal care and use committee approved all experimental procedures. Experiments were performed on six female apoE−/− mice (Charles River, Maastricht, the Netherlands), which were put on a Western-type diet (0.21% cholesterol) when they reached an age of 12 weeks. Three weeks after start of the diet, a tapered cast (Promolding BV., The Hague, the Netherlands) was surgically placed around the right carotid artery to induce plaque formation on both sides of the cast [5]. The inner diameter of the cast ranges from 500 μm upstream to 250 μm downstream, and the cast was placed around the right carotid artery well separated (at least 1 mm) from the bifurcation. Six weeks after surgery, MRI measurements were performed.

Histology

Both the upstream and downstream plaques were sectioned into 8-μm serial sections perpendicular to the vessel direction. Sections were stained with Hematoxylin & Eosin, Oil Red O for lipids and Picrosirius Red for collagen (analyzed with a circular polarizing filter) at 80-μm intervals. Bright-field microscopy was performed with a Zeiss Axio Observer Z1 microscope (Carl Zeiss, Inc.).

MRI

In vivo MRI was performed with a 9.4 T horizontal-bore animal scanner (Bruker BioSpin, Ettlingen, Germany) running Paravision 5 software. The mice were initially anesthetized with 3% isoflurane in medical air and maintained with 1–2% isoflurane during the MRI experiments. The mice were placed in a custom-made cradle, which contained a heating pad with a temperature of approximately 37°C to sustain the mouse body temperature and placed in the MRI scanner within a 3.5-cm-diameter quadrature birdcage RF coil. Respiration and heart rate were monitored with a balloon sensor and ECG trigger leads, connected to an ECG/respiratory unit (Rapid Biomedical, Rimpar, Germany). The MRI protocols (N = 6 mice) consisted of time-of-flight MR angiography, T1- and T2-weighted imaging and phase-contrast velocity imaging. The total examination time including preparations and planning was approximately 2 h.

Time-of-flight MR angiography was done with a three-dimensional gradient-echo sequence. Sequence parameters were TR = 15 ms, TE = 2.5 ms, flip angle = 20°, FOV = $2.56 \times 2.56 \times 2.56$ cm^3, acquisition matrix = $256 \times 256 \times 256$, NA = 2, total scan time = 18 min. T1- and T2-weighted imaging in sagittal and transversal orientations was performed using a black-blood multi-slice spin-echo sequence. Black blood was achieved by placing two saturation slabs below and above the neck region saturating inflowing blood. Sequence parameters for T1-weighted imaging were TR = 800 ms, TE = 7.5 ms, FOV = 2.56×2.56 cm^2, acquisition matrix = 256×256, reconstruction matrix = 512×512, slice thickness = 0.5 mm, NA = 2, total scan time = 8 min. Sequence parameters for T2-weighted imaging were TR = 2000 ms, TE = 20 ms, FOV = 2.56×2.56 cm^2, acquisition matrix = 256×256, reconstruction matrix = 512×512, slice thickness = 0.5 mm, NA = 2, total scan time = 20 min. T1- and T2-weighted scans were triggered to heart and respiratory signals to suppress motion artifacts. Phase-contrast velocity imaging was performed using an ECG-triggered gradient-echo sequence with bipolar gradient pulses encoding for flow perpendicular to the imaging slice. To enhance the signal-to-noise, a Gd-based blood pool agent (paramagnetic micelles, dose of 50 μmol Gd per kg body weight) was intravenously injected prior to phase-contrast

velocity imaging [7]. We would like to stress that the purpose of this blood pool agent was solely to lower the T1 of the blood to enhance the signal-to-noise and was not intended to provide enhanced plaque contrast. Sequence parameters were as follows: TR = 12 ms, TE = 5 ms, flip angle = 30°, FOV = 2.56 × 2.56 cm^2, acquisition matrix = 384 × 384, reconstruction matrix = 512 × 512 (pixel size = 50 × 50 μm^2), slice thickness = 0.5 mm, NA = 6, V$_{enc}$=100 cm/s, number of frames = 9. Flow encoding was repeated twice with encoding gradients in opposite direction to compensate for background phase caused by field inhomogeneities. The sequence was triggered by the QRS-complex and repeated three times with starting delays of 1, 5 and 9 ms, respectively, resulting in 27 time frames through the cardiac cycle with a time resolution of 4 ms. Total scan time for a single-slice phase-contrast velocity image was approximately 18 min. Two slices were measured, one downstream and the other upstream to the cast (see Fig. 3a).

Image analysis

Maximum intensity projections (MIP) of the time-of-flight angiography images were made using OsiriX 3.5.1 (www. osirix-viewer.com) software. Flow velocity images were processed in Mathematica 7 (Wolfram Research, Inc.). First four regions of interest (ROI) were manually drawn to select the lumen of the left and right carotid arteries in the downstream and upstream anatomical images. Reported flow velocities in the arteries are the mean velocity of the 10% pixels with the highest velocity within the ROIs at every time point through the cardiac cycle. Flow velocities of six mice were averaged. Subsequently, the flow velocity profiles of the 3 time points in the cardiac cycle with the highest flow were fitted with a quadratic polynomial. The wall shear stress (WSS) was determined from WSS $= \mu \frac{dv}{dr}$, with v the blood velocity at the carotid artery wall and mouse blood viscosity $\mu = 10$ mPa s [8]. WSS from the 3 time points and six mice was averaged.

Statistical analysis

Differences in the flow velocities as function of time in the cardiac cycle between left and right carotid arteries were tested using a two-way analysis of variance (factors: left or right carotid artery and time; significance level $P < 0.05$) with Bonferroni post hoc test. Differences in lumen diameter and wall shear stress were tested using a Student's t-test (significance level $P < 0.05$). Statistical analyses were performed in Mathematica 7 (Wolfram Research, Inc.).

Results

MR angiography

Figure 1 displays a MIP of a time-of-flight angiography measurement of the neck area of a representative mouse. A movie of this MIP rotating about the H-F axis can be found in the supplementary content. The arrow indicates the position of the cast in the right carotid artery. The arteries in this MR angiography image are bright because magnetically unsaturated blood from the heart enters via the aorta into the carotid arteries and the imaging volume. The presence of high blood signal intensity downstream to the cast extending beyond the carotid bifurcation and further, therefore, confirms that the vessel is still patent. Upon closer inspection, the tapered shape of the cast can be appreciated in the image, which confirms correct placement of the cast around the right carotid artery. The three-dimensional angiography images were also useful to locate slices perpendicular to the carotid arteries for anatomical and flow velocity measurements.

Histology

To confirm the plaque characteristics, upstream and downstream plaques were evaluated by histology, as presented in Fig. 2. In agreement with the observations by Cheng et al. [5], the upstream plaques (Fig. 2a) showed characteristics
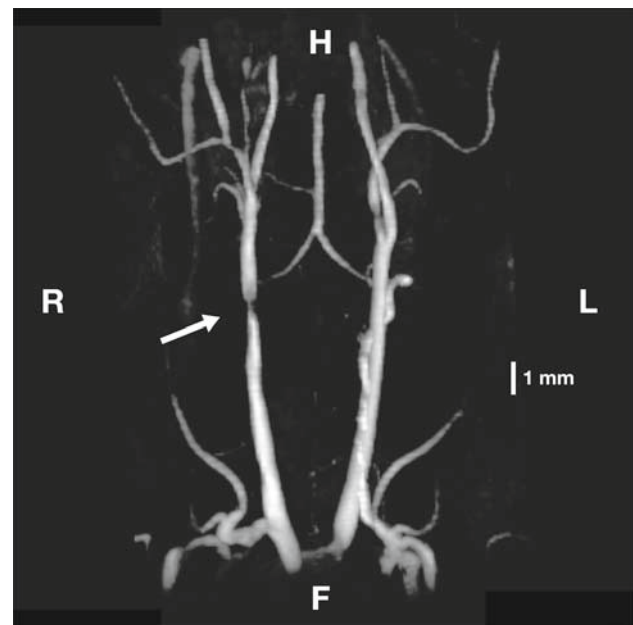

Fig. 1 Maximum intensity projection of the three-dimensional time-of-flight MR angiography. The *arrow* indicates the position of the cast (H = head, F = feet, R = right, L = left). A movie of the MIP rotating about the H-F axis can be found in the supplementary content

Fig. 2 Histological sections of right carotid arteries. **a** Upstream to the cast. **b** Downstream to the cast. Sections were stained with Hematoxylin & Eosin, Oil Red O for lipids, and Picrosirius Red for collagen. The scale bar equals 200 µm
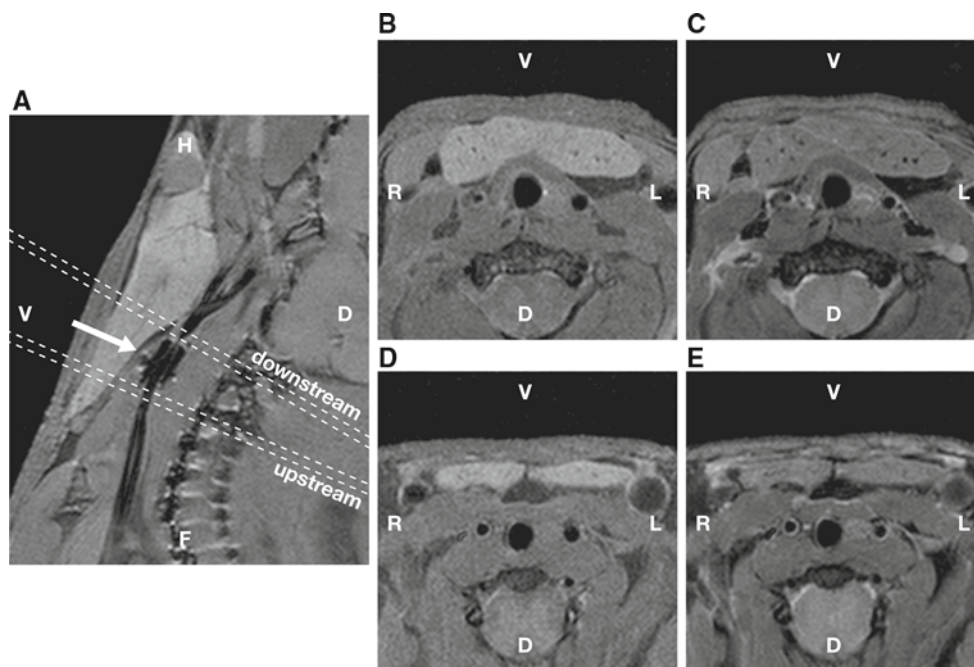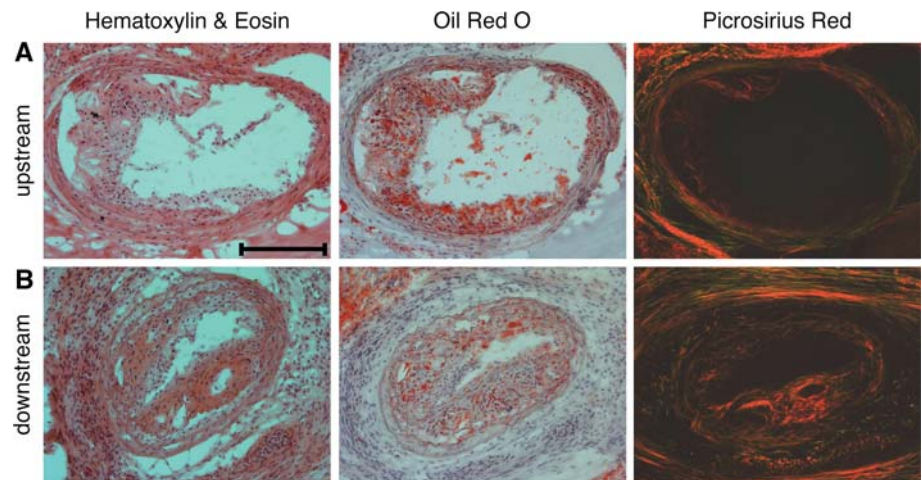

Fig. 3 T1- and T2-weighted imaging of the neck region of the mouse. **a** T1-weighted image in sagittal orientation. The position of the cast is indicated with the *arrow*. The *dashed lines* indicate the position of transversal upstream and downstream slices. Image size is $12 \times 15\,\text{mm}^2$. **b** T1-weighted transversal slice downstream. **c** T2-weighted transversal slice downstream. **d** T1-weighted transversal slice upstream. **e** T2-weighted transversal slice upstream. Image size of B-E is $10 \times 10\,\text{mm}^2$ (H = head, F = feet, V = ventral, D = dorsal, L = left, R = right)

of a vulnerable phenotype, with high lipid and low collagen content, while the downstream plaques (Fig. 2b) had characteristics of a more stable phenotype, with lower lipid and higher collagen content.

T1- and T2-weighted MRI

Figure 3a displays a sagittal T1-weighted MR image of the right carotid artery. Signal of inflowing blood was magnetically saturated and therefore the lumen of the carotid artery appears black. The position of the cast is indicated with the arrow. Inside the cast, the arterial wall is weakly visible. The cast itself is MRI silent and therefore appears black on these images, which facilitated accurate placement of transversal (perpendicular to the arteries) imaging slices. In Fig. 3b–e, transversal T1- and T2-weighted images are shown of slices placed directly upstream and downstream to the cast as indicated by the dashed lines in Fig. 3a. In many instances, the intensity of the right carotid artery wall, particularly in the T2-weighted images, was higher than
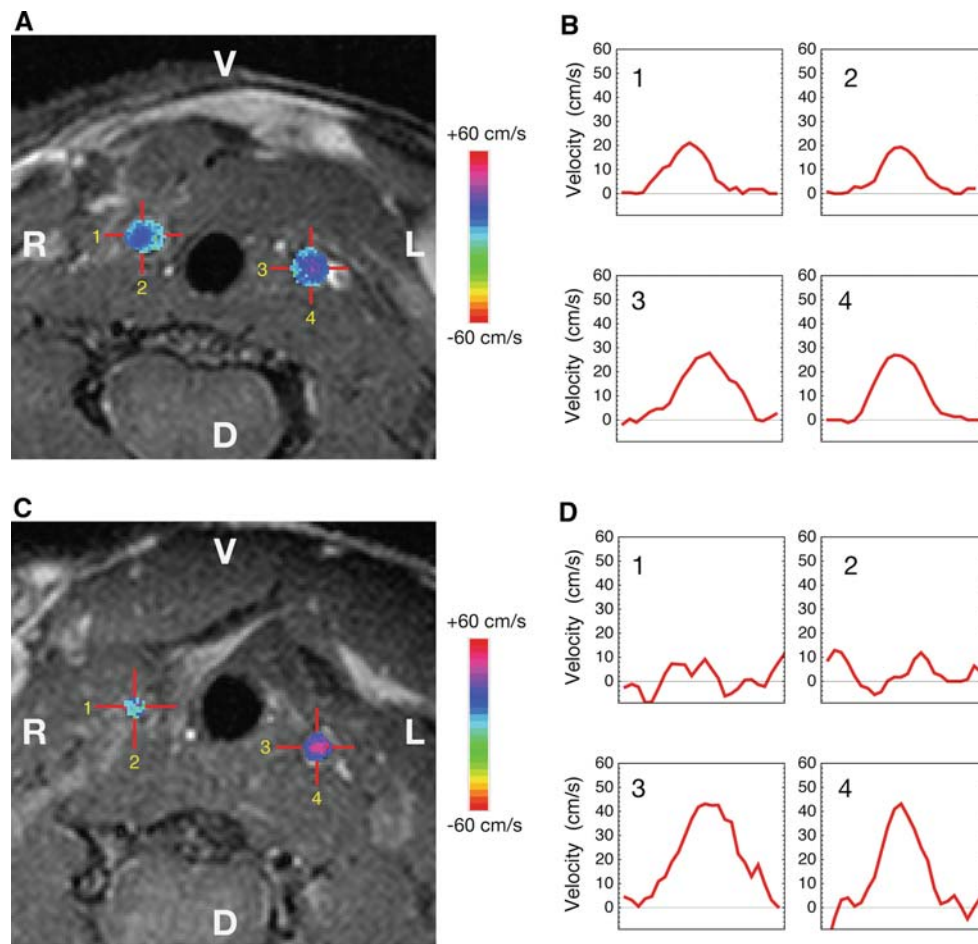
Fig. 4 T1-weighted images with color-coded maximum flow velocities in the left and right carotid arteries. **a**, **b** Upstream to the cast. **c**, **d** Downstream to the cast (V = ventral, D = dorsal, R = right, L = left). Image size in **a** and **c** is 7 × 7 mm². Panels **b** and **d** show the flow profiles along the *red lines* in the corresponding panels **a** and **c**, indicated by *1*, *2*, *3*, and *4*. *Red lines* have a length of 1.2 mm. Movies of the flow velocities in the carotid arteries through the cardiac cycle can be found in the supplementary content

surrounding muscle, which can be attributed to the presence of the atherosclerotic lesions. In the contralateral left carotid, artery signal of the vessel wall was essentially isointense with surrounding muscle. Nevertheless, contrast and resolution, particularly in slice direction (0.5 mm), were not sufficient to quantify plaque burden in these tiny arteries. Ex vivo histological analysis of carotid artery sections confirmed the presence of plaque in the upstream and downstream locations, with plaque characteristics as described by Cheng et al. [5]. The average ($N = 6$ mice) diameters of the carotid artery lumen at the four positions, i.e., right carotid upstream, right carotid downstream, left carotid upstream and left carotid downstream, were 0.57 ± 0.12, 0.41 ± 0.17, 0.54 ± 0.11 and 0.49 ± 0.08 mm, respectively. While there were variations between mice, the average right carotid artery lumen at downstream position proved significantly different from the upstream position (significance level $P < 0.05$).

Phase-contrast velocity imaging

Flow measurements were analyzed in the left and right carotid arteries. Figure 4a and c show examples of T1-weighted images at upstream and downstream locations to the cast, with color-coded maximum flow velocities in the left and right carotid arteries. The panels in Fig. 4b and d show the flow profiles along the red lines numbered 1–4 in the corresponding Fig. 4a and c. Movies of the flow in the carotid arteries through the full cardiac cycle can be found in the supplementary content. The flow profiles display a quadratic shape, indicative for laminar flow, except for the right carotid artery at downstream position, where the apparent flow is low and irregular.

In Fig. 5, the flow velocities as function of time through the cardiac cycle are shown. Flow in the left carotid artery, upstream as well as downstream positions, and the right carotid artery, downstream position only, peaked at about

Fig. 5 Flow velocities as function of time in the cardiac cycle. **a** Upstream to the cast. **b** Downstream to the cast. *Solid squares* are from the right carotid artery, whereas *solid circles* from the left carotid artery. Velocity is presented as mean±standard deviation from six mice
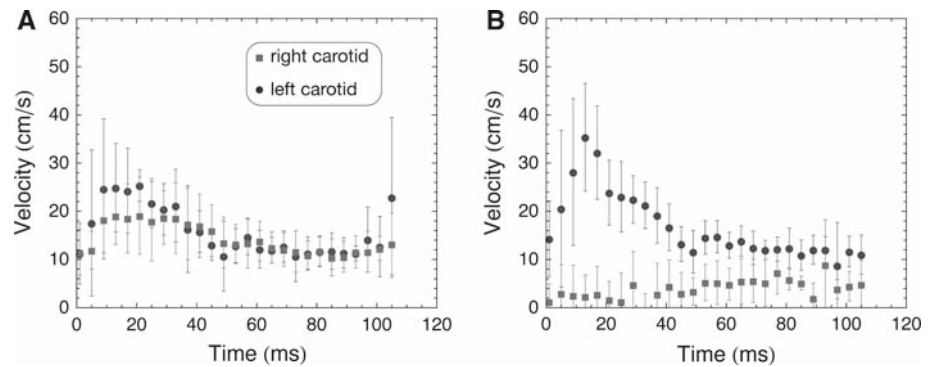
15 ms after the R-top. The maximum flow velocity at upstream positions (Fig. 5a) seemed somewhat higher in the left carotid artery, although the difference was not statistically significant. At the downstream position of the left carotid artery, flow displayed a similar profile as in the right carotid artery except for higher maximum flow velocity. At the downstream position of the right carotid artery, the apparent flow was consistently low. The apparent flow during the systolic phase (approximately first 50 ms) was even somewhat lower than during the diastolic phase (starting at about 50 ms).

WSS at maximum flow velocity is plotted in Fig. 6. The average ($N = 6$ mice) WSS at the three locations, i.e., right carotid upstream, left carotid upstream and left carotid downstream, was 11.2 ± 5.2, 17.5 ± 7.5 and 24.5 ± 10.9 Pa, respectively. WSS in the three locations was significantly different (significance level $P < 0.05$). WSS in the right carotid artery downstream position could not be determined as the flow profile displayed an irregular non-laminar flow profile.

Fig. 6 Box whisker plots of the wall shear stress (WSS) at maximum flow for the right carotid artery upstream location and the left carotid artery, upstream and downstream locations. The *solid line* represents the mean; the *dashed line* the median. *,† Significantly different ($p < 0.05$)

Discussion

Various imaging modalities have been used to study plaque formation and characteristics in the apoE−/− mouse model [9–11]. MRI has been used to study plaque burden in the abdominal aorta of mice [12–15], and recently, several studies have focused on pre-clinical evaluation of novel targeted contrast agents to identify molecular fingerprints of plaque vulnerability [7,16–20]. The apoE−/− mouse with tapered cast represents an extremely attractive model of atherosclerosis as it allows for studying plaques with both stable and vulnerable characteristics within one animal and within a single vascular segment. This study specifically focused on anatomical MRI characterization of the model and on quantification of flow velocities and wall shear stress. The latter is considered one of the key players in the development of plaque phenotype [2–4].

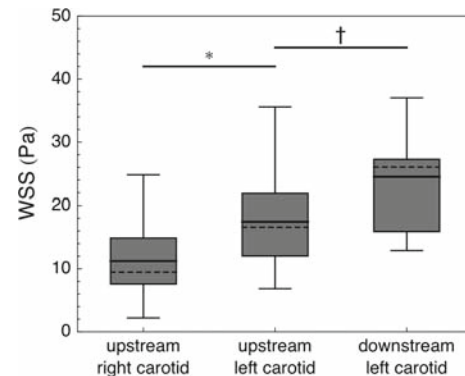MR angiography provided detailed images of the mouse neck vasculature, which were used to verify that the right carotid artery was still patent and to confirm correct placement of the cast. Additionally, they proved useful for planning imaging slices exactly perpendicular to the carotid arteries. Similar MR angiography has previously been used to provide details on the mouse vasculature [21–23]. Recently, a time-resolved three-dimensional angiography sequence was used to measure blood flow in the mouse carotid arteries [24]. This technique, however, only measures the averaged flow velocity within the carotid arteries and is therefore not suitable to provide details on the shape of the flow profile or the wall shear stress.

Our flow velocity measurements indicated that the maximum flow velocity in the right carotid artery was somewhat lower than the contralateral left carotid artery, which roughly scaled to the difference in wall shear stress. We found a maximum flow velocity in the carotid arteries of about 35 cm/s, which is in good agreement with the MRI study by Parzy et al. [25], who reported a vessel-averaged flow velocity of about 18 cm/s in the systolic heart phase. Maximum blood flow velocities up to 120 cm/s were reported at sites of mouse carotid artery plaque by means of pulse-wave Doppler [10]. However, these high values when compared to our studies could well be due to a larger degree of stenosis in

their mouse model. The apparent flow velocities in the right carotid artery downstream to the cast were consistently low with irregular flow profiles. Since total flow rate in the right carotid artery is preserved, the apparent flow velocities at this position do not represent total flow rates and are most probably caused by irregular non-laminar flow in this region. The wall shear stresses in the upstream region were 11.2 ± 5.2 and 17.5 ± 7.5 Pa for the right and left carotid arteries, respectively, which compares very well to 10 and 15 Pa determined by Doppler ultrasound measurements in the same model [5].

A limitation to the study is that it was not possible to confirm the oscillatory nature of the blood flow and the wall shear stress in the downstream location at the position of the stable plaque. The reason for this is twofold. First, the resolution in slice direction was 0.5 mm, which is likely not sufficient to reveal vortices or irregular flow of smaller dimensions directly after the cast. Second, we used a phase-contrast velocity imaging sequence in this study, which measures flow in slice direction only. High-resolution Doppler ultrasound could provide an alternative imaging modality to confirm oscillatory flow [10]. Nevertheless, because the total flow rate in the right carotid artery has to be preserved, the absence of a laminar flow profile in the downstream right carotid artery position actually is a strong indication that the flow is highly irregular there, providing indirect proof for the oscillatory nature of the flow.

In the future, the pre-clinical MRI protocols presented here can be used to evaluate novel treatment strategies and new molecular imaging contrast agents for specific imaging of plaque constituents. Additionally, one could consider developing a three-dimensional flow velocity imaging protocol for the mouse carotid arteries, providing a higher resolution along the arteries and enabling quantification of flow velocity profiles and wall shear stress at several positions upstream, in and downstream to the cast. The protocols presented here are not exclusively suitable for imaging the carotid arteries. They can be straightforwardly translated to study the role of flow and wall shear stress in the aortic arch and the abdominal aorta [26–28].

Conclusions

In conclusion, the apoE−/− mouse model of atherosclerosis with tapered cast around the carotid arteries was characterized using pre-clinical high-field MRI, with specific focus on the measurement of flow in view of its relevance to plaque development patterns. MR angiography showed that blood flow through the right carotid artery was preserved and revealed the tapered nature of the constriction. Laminar flow with low wall shear stress was measured at the position of the vulnerable plaque, upstream to the cast. Apparent flow velocities were low at the position of the stable plaque, down-

stream to the cast, which is consistent with the occurrence of vortices or an oscillatory nature of the flow.

References

1. Chien S (2008) Effects of disturbed flow on endothelial cells. Ann Biomed Eng 36(4):554–562
2. Pedersen EM, Oyre S, Agerbaek M, Kristensen IB, Ringgaard S, Boesiger P, Paaske WP (1999) Distribution of early atherosclerotic lesions in the human abdominal aorta correlates with wall shear stresses measured in vivo. Eur J Vasc Endovasc Surg 18(4):328–333
3. Buchanan JR, Kleinstreuer C, Truskey GA, Lei M (1999) Relation between non-uniform hemodynamics and sites of altered permeability and lesion growth at the rabbit aorto-celiac junction. Atherosclerosis 143(1):27–40
4. Stone PH, Coskun AU, Kinlay S, Clark ME, Sonka M, Wahle A, Ilegbusi OJ, Yeghiazarians Y, Popma JJ, Orav J, Kuntz RE, Feldman CL (2003) Effect of endothelial shear stress on the progression of coronary artery disease, vascular remodeling, and in-stent restenosis in humans: in vivo 6-month follow-up study. Circulation 108(4):438–444
5. Cheng C, Tempel D, van Haperen R, van der Baan A, Grosveld F, Daemen MJ, Krams R, de Crom R (2006) Atherosclerotic lesion size and vulnerability are determined by patterns of fluid shear stress. Circulation 113(23):2744–2753
6. Mulder WJ, Strijkers GJ, Vucic E, Cormode DP, Nicolay K, Fayad ZA (2007) Magnetic resonance molecular imaging contrast agents and their application in atherosclerosis. Top Magn Reson Imaging 18(5):409–417
7. Mulder WJ, Strijkers GJ, Briley-Saboe KC, Frias JC, Aguinaldo JG, Vucic E, Amirbekian V, Tang C, Chin PT, Nicolay K, Fayad ZA (2007) Molecular imaging of macrophages in atherosclerotic plaques using bimodal PEG-micelles. Magn Reson Med 58(6):1164–1170
8. Windberger U, Bartholovitsch A, Plasenzotti R, Korak KJ, Heinze G (2003) Whole blood viscosity, plasma viscosity and erythrocyte aggregation in nine mammalian species: reference values and comparison of data. Exp Physiol 88(3):431–440
9. Isobe S, Tsimikas S, Zhou J, Fujimoto S, Sarai M, Branks MJ, Fujimoto A, Hofstra L, Reutelingsperger CP, Murohara T, Virmani R, Kolodgie FD, Narula N, Petrov A, Narula J (2006) Noninvasive imaging of atherosclerotic lesions in apolipoprotein E-deficient and low-density-lipoprotein receptor-deficient mice with annexin A5. J Nucl Med 47(9):1497–1505
10. Ni M, Zhang M, Ding SF, Chen WQ, Zhang Y (2008) Micro-ultrasound imaging assessment of carotid plaque characteristics in apolipoprotein-E knockout mice. Atherosclerosis 197(1):64–71
11. Nahrendorf M, Zhang H, Hembrador S, Panizzi P, Sosnovik DE, Aikawa E, Libby P, Swirski FK, Weissleder R (2008) Nanoparticle PET-CT imaging of macrophages in inflammatory atherosclerosis. Circulation 117(3):379–387

12. Fayad ZA, Fallon JT, Shinnar M, Wehrli S, Dansky HM, Poon M, Badimon JJ, Charlton SA, Fisher EA, Breslow JL, Fuster V (1998) Noninvasive in vivo high-resolution magnetic resonance imaging of atherosclerotic lesions in genetically engineered mice. Circulation 98(15):1541–1547

13. Worthley SG, Helft G, Fuster V, Zaman AG, Fayad ZA, Fallon JT, Badimon JJ (2000) Serial in vivo MRI documents arterial remodeling in experimental atherosclerosis. Circulation 101(6):586–589

14. Choudhury RP, Aguinaldo JG, Rong JX, Kulak JL, Kulak AR, Reis ED, Fallon JT, Fuster V, Fisher EA, Fayad ZA (2002) Atherosclerotic lesions in genetically modified mice quantified in vivo by non-invasive high-resolution magnetic resonance microscopy. Atherosclerosis 162(2):315–321

15. Dietrich T, Hucko T, Bourayou R, Jahnke C, Paetsch I, Atrott K, Stawowy P, Grafe M, Klein C, Schnackenburg B, Fleck E, Graf K (2009) High resolution magnetic resonance imaging in atherosclerotic mice treated with ezetimibe. Int J Cardiovasc Imaging 25:827–836

16. Mulder WJ, Douma K, Koning GA, van Zandvoort MA, Lutgens E, Daemen MJ, Nicolay K, Strijkers GJ (2006) Liposome-enhanced MRI of neointimal lesions in the ApoE-KO mouse. Magn Reson Med 55(5):1170–1174

17. Nahrendorf M, Jaffer FA, Kelly KA, Sosnovik DE, Aikawa E, Libby P, Weissleder R (2006) Noninvasive vascular cell adhesion molecule-1 imaging identifies inflammatory activation of cells in atherosclerosis. Circulation 114(14):1504–1511

18. Kelly KA, Nahrendorf M, Yu AM, Reynolds F, Weissleder R (2006) In vivo phage display selection yields atherosclerotic plaque targeted peptides for imaging. Mol Imaging Biol 8(4):201–207

19. McAteer MA, Schneider JE, Ali ZA, Warrick N, Bursill CA, von zur Muhlen C, Greaves DR, Neubauer S, Channon KM, Choudhury RP (2008) Magnetic resonance imaging of endothelial adhesion molecules in mouse atherosclerosis using dual-targeted microparticles of iron oxide. Arterioscler Thromb Vasc Biol 28(1):77–83

20. Burtea C, Laurent S, Murariu O, Rattat D, Toubeau G, Verbruggen A, Vansthertem D, Vander Elst L, Muller RN (2008) Molecular imaging of alpha v beta3 integrin expression in atherosclerotic plaques with a mimetic of RGD peptide grafted to Gd-DTPA. Cardiovasc Res 78(1):148–157

21. Beckmann N (2000) High resolution magnetic resonance angiography non-invasively reveals mouse strain differences in the cerebrovascular anatomy in vivo. Magn Reson Med 44:252–258

22. Yang YM, Feng X, Yao ZW, Tang WJ, Liu HQ, Zhang L (2008) Magnetic resonance angiography of carotid and cerebral arterial occlusion in rats using a clinical scanner. J Neurosci Methods 167(2):176–183

23. Jacoby C, Böring Y, Beck A, Zernecke A, Aurich V, Weber C, Schrader J, Flögel U (2008) Dynamic changes in murine vessel geometry assessed by high-resolution magnetic resonance angiography: a 9.4T study. J Magn Reson Imaging 28(3):637–645

24. Miraux S, Franconi J, Thiaudière E (2006) Blood velocity assessment using 3D bright-blood time-resolved magnetic resonance angiography. Magn Reson Med 56(3):469–473

25. Parzy E, Miraux S, Franconi JM, Thiaudière E (2009) In vivo quantification of blood velocity in mouse carotid and pulmonary arteries by ECG-triggered 3D time-resolved magnetic resonance angiography. NMR Biomed 22(5):532–537

26. Rensen SS, Niessen PM, van Deursen JM, Janssen BJ, Heijman E, Hermeling E, Meens M, Lie N, Gijbels MJ, Strijkers GJ, Doevendans PA, Hofker MH, De Mey JG, van Eys GJ (2008) Smoothelin-B deficiency results in reduced arterial contractility, hypertension, and cardiac hypertrophy in mice. Circulation 118(8):828–836

27. Herold V, Wellen J, Ziener CH, Weber T, Hiller KH, Nordbeck P, Rommel E, Haase A, Bauer WR, Jakob PM, Sarkar SK (2009) In vivo comparison of atherosclerotic plaque progression with vessel wall strain and blood flow velocity in apoE(−/−) mice with MR microscopy at 17.6 T. Magn Reson Mater Phys 22(3):159–166

28. Zhao X, Pratt R, Wansapura J (2009) Quantification of aortic compliance in mice using radial phase contrast MRI. J Magn Reson Imaging 30(2):286–291